Bioconjugate Chemistry

Article

Cite This: Bioconjugate Chem. XXXX, XXX, XXX−XXX

pubs.acs.org/bc

Signal Amplification for Imaging Mass Cytometry

Rahul Rana,[†] Rodolfo F. Gómez-Biagi,[‡] Jay Bassan,[†,§] and Mark Nitz*[,†]

[†]Department of Chemistry, University of Toronto, 80 St. George Street, Toronto, ON M5S 3H6, Canada

[‡]SPARC BioCentre—The Hospital for Sick Children, The Peter Gilgan Centre for Research and Learning, 686 Bay Street, 21st Floor, Toronto, ON M5G 0A4, Canada

[§]BIMDAQ Ltd, 9 Lessness Avenue, Bexleyheath DA7 5SH, United Kingdom

Supporting Information

ABSTRACT: An enzyme-catalyzed reporter deposition stain has been developed for Imaging Mass Cytometry (IMC). The reagent consists of an alkaline phosphatase substrate tethered to a tellurophene which serves as reporter group for mass cytometry. Upon phosphate hydrolysis, a quinone methide is released which covalently labels local nucleophiles. This strategy is a useful complement to heavy isotope antibody conjugates as it facilitates signal amplification for low-abundance biomarker detection. The workflow is conveniently integrated with standard IMC antibody staining to allow multiparametric antigen detection.

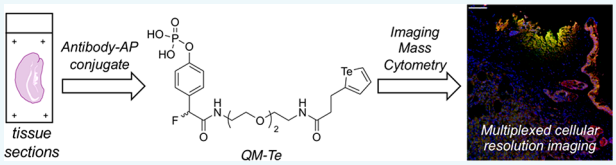

Mass cytometry (MC) has enabled highly multiparametric single-cell analysis (>40 parameters/cell) which has yielded insight into disease and therapy.[1,2] MC uses heavy isotope mass tags tethered to bioaffinity reagents to identify biomarkers. The heavy isotopes are quantified through single-cell inductively coupled plasma mass spectrometry (ICP-MS) analysis in a workflow analogous to flow cytometry. The mass resolution of the ICP-MS and the large number of available heavy isotopes allow highly parametrized experiments with minimal complications due to signal overlap.[3] Similarly, imaging mass cytometry (IMC) couples these high-dimensional measurements with 2-D resolution via laser ablation of immunohistochemical and immunocytochemical sections.[4] IMC has been successfully used to study immunophenotypic states,[5] study drug distribution in tissues,[6] and quantify mRNA transcripts.[7]

At present, the catalogue of MC- and IMC-compatible stains consists of antibodies conjugated with metal-chelating polymers which bind, with high affinity, the lanthanide series as well as indium, yttrium, palladium, and bismuth.[8−10] Beyond these bioaffinity reagents, small-molecule MC-compatible stains have been validated for multiple applications. For example, DNA cycle studies have been performed using 5-iodo-2′-deoxyuridine (IdU), and palladium and platinum complexes have been used as cell barcoding and live dead stains.[11,12] We have introduced tellurophenes as versatile functionalities to incorporate into small-molecule MC-compatible reagents.[13] Using tellurophenes, probes have been developed to follow tumor hypoxia,[14] protein synthesis,[15] and cellular senescence.[16]

While the benefits of highly parametrized assays are evident, MC and IMC are less sensitive than fluorescence, and methods to improve the detection of low-abundance antigens would expand the scope of their applications. Recently, nanoparticle reagents have been introduced to improve the sensitivity of MC experiments, and this approach shows promise with primary antibody conjugates.[17] Here we sought to introduce an IMC-compatible enzyme amplification strategy which would improve the sensitivity of IMC while not compromising mass channels commonly used with antibody conjugates. An enzyme amplification strategy would be compatible with standard secondary immunohistochemistry (IHC) antibody protocols, allowing direct translation and comparison between existing analyses and IMC analysis. In addition, primary antibodies not bearing a mass tag can readily be incorporated into characterized commercial MaxPar libraries.

AP-conjugates are ubiquitous in immunoassays with numerous well-characterized synthetic substrates.[18,19] Latent quinone methide (QM) derivatives, developed originally as AP covalent inhibitors,[20,21] have been used to covalently label phosphatases in solution for visualization.[22−26] Kinetic analysis and product analysis of QMs generated enzymatically suggest these products diffuse away from the enzymes active site and label local nucleophiles.[16,27] In the case of an AP antibody conjugate, the QM released will be immobilized by local nucleophiles, in close proximity to the site of QM generation (Scheme 1). Provided adequate turnover can be realized, a significant degree of signal amplification with minimal diffusion can be achieved. This improves both the limit of detection and dynamic range of signal. Thus, we developed a latent-QM AP substrate bearing a tellurophene (QMTe) as a universal reagent for use with AP-conjugates in IMC.

Polaske et al. reported the use of *o*-monofluoromethyl- and *o*-difluoromethyl-substituted fluorescent AP substrates as QM precursors for IHC.[28] While both reagents were able to detect

Received: August 19, 2019
Revised: October 9, 2019

DOI: 10.1021/acs.bioconjchem.9b00559
Bioconjugate Chem. XXXX, XXX, XXX−XXX

Scheme 1. Mechanism of Amplified Labelling by QMTe

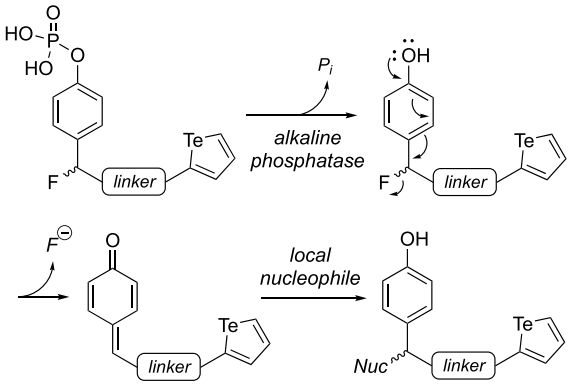

Scheme 2. Synthetic Preparation of QMTe[a]

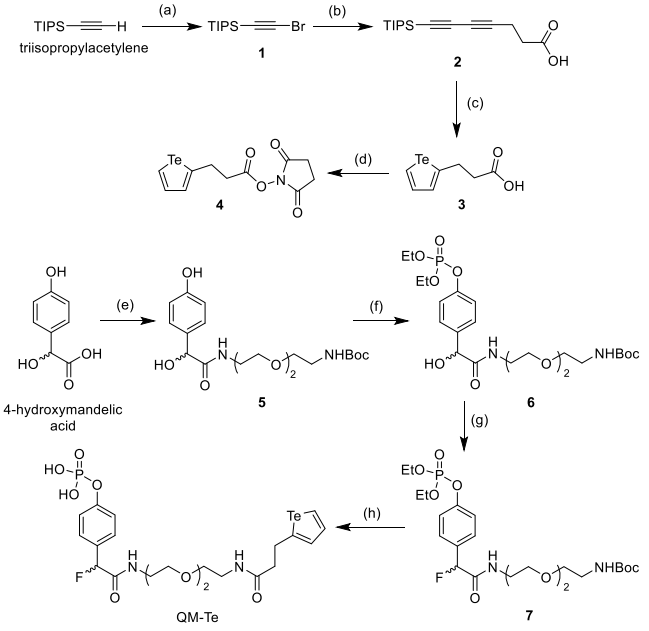

[a]Reagents and conditions: (a) NBS, $AgNO_3$, acetone, rt, quantitative; (b) 4-pentynoic acid, CuCl, $NH_2OH{\cdot}HCl$, 30% aq. $BuNH_2$, 0 °C, 70%; (c) i. TBAF, (1.0 M in THF), THF 50 °C, ii. Te^0, $NaBH_4$, $EtOH/H_2O$, 60 °C, 63%; (d) *N*-hydroxysuccinimide, T_3P (50% wt. EtOAc), DIPEA, THF, 0 °C, 82%; (e) *N*-Boc- 2,2′-(ethylenedioxy)-diethylamine, EDC, HOBt, DMF, rt, 84%; (f) diethylchlorophosphate, NEt_3, DCM, 0 °C, 66%; (g) XtalFluor-E, NEt_3.HF, DCM, −78 °C, 84%; (h) i. TMSBr, DCM 0 °C, ii. **4**, NEt_3, DMF, rt (18%).

antigens via an AP secondary antibody, the difluoromethyl analogue exhibited higher nonspecific staining. This was attributed to the longer half-life of the difluoromethylphenol, which allows diffusion from the site of QM generation compromising resolution. The *o*-monofluoromethyl QM precursors gave better resolution, but *o*-monofluoromethyl is known to be chemically less stable as it is prone to solvolysis and undesirable side reactions with thiols and other nucleophilic buffer components.[29] Furthermore, from a synthetic perspective, the *o*-monofluoromethyl group is susceptible to displacement by the *o*-phosphate during final deprotection, resulting in a cyclic phosphodiester byproduct and reduced yields. To circumvent these issues, we prepared *p*-phosphobenzylic fluoride scaffold, a latent trapping group that undergoes a 1,6-elimination mechanism.[30,31]

The tellurophene mass reporter group was synthesized according to previous reports with minor modifications (Scheme 2).[16] After Cadiot−Chodkiewicz coupling of **1** with 4-pentynoic acid, diyne **2** was deprotected with tetrabutylammonium fluoride. The crude mixture was treated immediately with a solution of sodium hydrogen telluride generated from excess sodium borohydride and tellurium metal. The major isolated product, 3-(tellurophen-2-yl)propanoic acid (**3**), was activated to prepare the corresponding *N*-hydroxysuccinimide ester **4**. The AP substrate coupling partner was synthesized in four steps. Briefly, *N*-Boc-2-(2-aminoethoxy)ethylamine was coupled to 4-hydroxymandelic acid to afford amide **5**. The phosphate recognition head was then installed on the phenol using diethylchlorophosphate, yielding intermediate **6**. We screened several fluorination conditions and found XtalFluor-E gave satisfactory yields of **7**. Trimethylsilyl bromide was used to cleave the phosphodiethyl ester and *N*-Boc groups, followed by coupling with **4**. QMTe was purified and obtained in 18% over two steps.

Prior to developing staining protocols, we investigated the turnover of QMTe by AP. Time course inhibition studies using *p*-nitrophenolphosphate to monitor AP activity showed that increasing concentrations of QMTe (0 to 1 mM) gave no significant AP inhibition over 1 h incubations with near complete probe hydrolysis (Supporting Information Figure S1). These results suggested significant amplification could be achieved as both the QMTe concentrations and incubation period were greater than those used in comparable IHC staining protocols.[28] To gain further insight into the fate of the quinone methide, AP-catalyzed turnover of QMTe was carried out in TRIS buffer, and the products were analyzed by LC-MS (Supporting Information Figure S2). The major product peak observed was consistent with a QM-TRIS buffer adduct suggesting the dephosphorylated product leaves the enzyme active site and reacts with local nucleophiles.

To evaluate staining properties of QMTe, commercial reference standard sections of paraffin-embedded cell line cores with negative, low, medium, and high expression levels of PD-L1 (CD274) were stained with a rabbit-anti-PD-L1 primary antibody followed by either a goat-antirabbit-AP and QMTe or a goat-antirabbit-^{175}Lu MaxPar secondary antibody. The sections were then analyzed by IMC.

While both methods were unable to discriminate between negative and low expression PD-L1 cell cores, significant signal (>2 count average) was observed in these samples with the QMTe protocol. Control experiments suggest that the signal observed in the PD-L1(−) sample is due to nonspecific binding of the GAR-AP conjugate. Experiments are ongoing to limit this background signal to further improve the antigen detection limit. However, with the current protocol, clear discrimination between the low and medium expression levels were observed using QMTe which could not be discriminated by current MaxPar reagents (Figure 1). Both detection antibodies were able to distinguish between medium and high expression levels, but the absolute values measured from QMTe are ∼100× higher than those from MaxPar labeling, indicating appreciable signal amplification. Additionally, the ratios of PDL1(+++) to PDL(−) signals for both stains are similar (approximately 40), suggesting QMTe does not disproportionately label off-target antigens. Taken together, these data support that QMTe is able to label its target antigen in a concentration-dependent manner with sensitivity at better than current secondary detection IMC methods.

DOI: 10.1021/acs.bioconjchem.9b00559
Bioconjugate Chem. XXXX, XXX, XXX−XXX

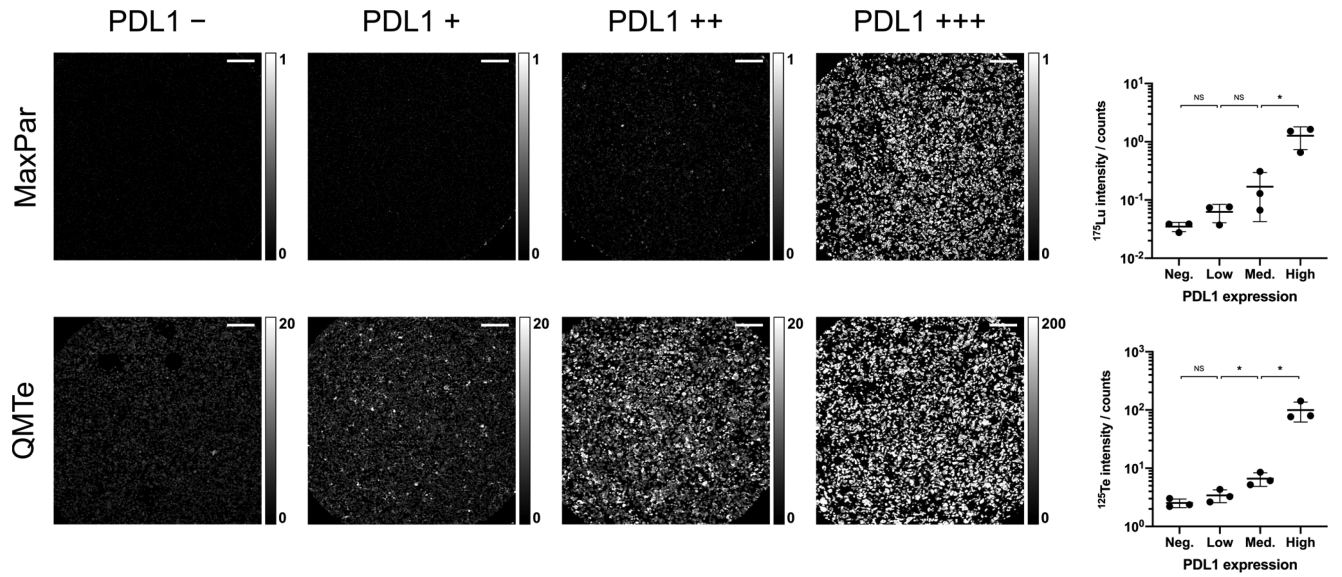

Figure 1. IMC images goat anti-rabbit-^{175}Lu(MaxPar) or ^{125}Te (QMTe) channels from PD-L1 negative (−), low (+), medium (++), or high (+++) slides. Median cellular labeling of segmented cells quantified ^{175}Lu or ^{125}Te counts accordingly. Three independent PD-L1 standard slides were stained; each represented data points. * = $p < 0.05$, NS = $p > 0.05$. Scale bar = 200 μm.

To validate the labeling specificity of QMTe for AP immunocomplexes, staining in the presence and absence of the AP-secondary antibody was performed. In this case, a different tissue source and target antigen were selected to evaluate the utility of QMTe across varied histological samples where MaxPar primary stains are not commercially available. Accordingly, we selected hornerin (HRNR), a member of the S100 family of extracellular matrix proteins.[32] Relative to normal pancreatic vasculature, HRNR expression is elevated in pancreatic ductal carcinoma models.[33] A pair of PANC-1 xenograft sections from mice were stained with anti-HRNR primary antibody and a combination of MaxPar ^{175}Lu and AP goat-antirabbit secondary antibodies or MaxPar ^{175}Lu secondary antibody alone; both sections were stained with QMTe. Pixelwise quantification showed good positive correlation between ^{175}Lu and ^{125}Te in the presence of both secondary antibodies, further confirming that our strategy labels the target antigen specifically. Low background levels of staining were observed with QMTe in the absence of the AP-conjugate secondary, demonstrating selective amplification only in the presence of AP-conjugate antibodies (Figure 2).

To demonstrate the use of QMTe in a typical IMC experimental workflow, we analyzed formalin-fixed paraffin-embedded sections of HCT116 xenograft tumors. Using QMTe we sought to visualize the localization of carbonic anhydrase IX (CAIX), a protein known to correlate with hypoxia in solid tumors, which is found on the border between necrotic and viable tissue.[34,35] The staining intensity using QMTe and AP-secondary antibody was compared to staining with the MaxPar ^{175}Lu secondary antibody as described above. With both secondary detection methods, CAIX staining displays the expected morphology of localization to hypoxic tumor regions close to necrosis, but QMTe offered stronger median signal intensity. Comparing CAIX staining between protocols, using DNA (^{193}Ir) signal as an internal standard for tissue thickness, we observed a 100-fold increase in staining intensity with QMTe over the MaxPar secondary antibody (Figure 3).

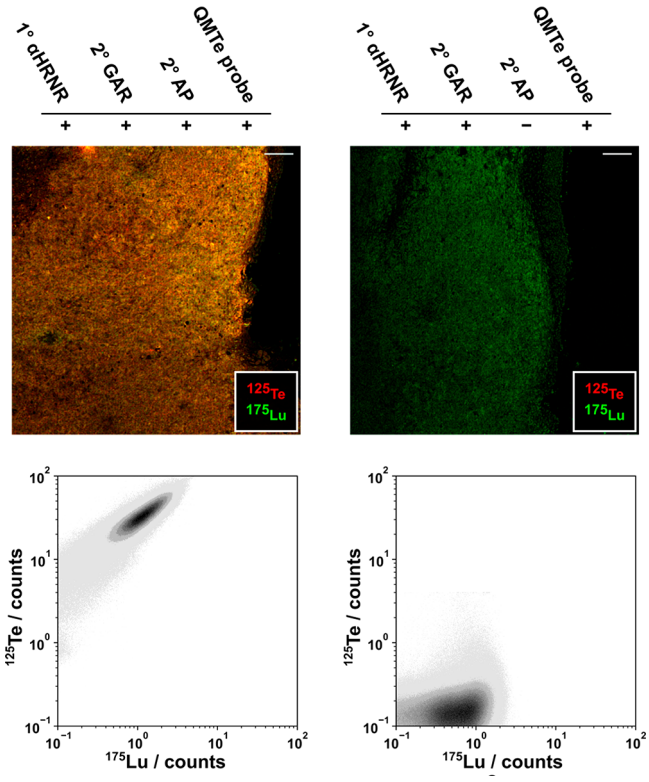

Figure 2. QMTe labeling is specific to AP-conjugates. (Top): two PANC-1 xenograft sections stained with a rabbit antihornerin primary antibody. Both sections stained with a goat antirabbit ^{175}Lu (MaxPar) antibody, but only the left section was stained with an antirabbit-AP. Both sections were exposed to the QMTe probe. Scale bars 200 μm. (Bottom): bivariate histograms showing pixelwise ^{175}Lu counts against ^{125}Te counts.

To demonstrate that QMTe is fully compatible with typical IMC workflows, we had stained the same HCT116 tissue sections before QMTe labeling with antibodies against epithelial cell adhesion molecule (EpCAM, ^{144}Nd), pan-keratin

DOI: 10.1021/acs.bioconjchem.9b00559
Bioconjugate Chem. XXXX, XXX, XXX−XXX

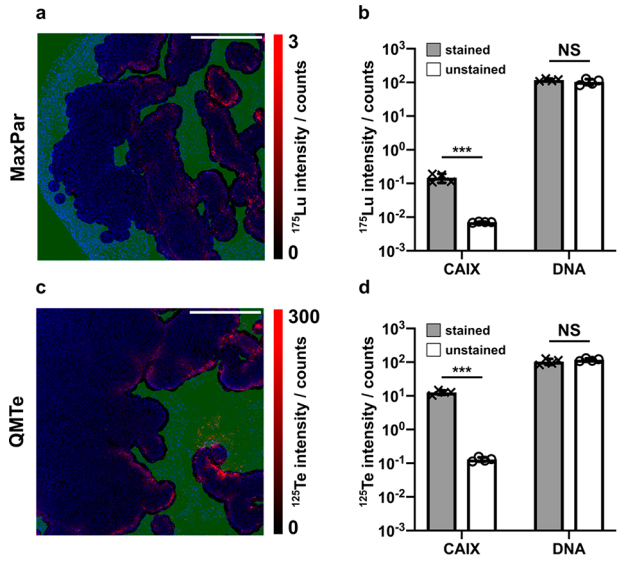

Figure 3. QMTe labels CAIX without loss of morphological information. (a) False color IMC image of HCT116 xenograft tumor section stained for DNA (^{193}Ir, blue) and CAIX (^{175}Lu MaxPar, red). Necrotic tumor regions are masked in green. (b) Single-cell segmented quantification of ^{175}Lu labeling of CAIX in four images using DNA as an internal control for the thickness of tissue. (c) Similar image to (a), instead showing CAIX as ^{125}Te signal from QMTe staining. (d) Quantification of QMTe labeling of CAIX in four images using DNA as an internal control for the thickness of tissue. Unstained slides for MaxPar were not stained with QMTe and vice versa and represent background signal. Mean and standard deviations are shown. *** = $p < 0.001$, NS = $p > 0.05$. Scale bars 500 μm.

(^{162}Dy), Ki67 (^{168}Er), and vascular endothelial growth factor (VEGF, ^{163}Dy). After QMTe labeling, DNA was also stained (^{193}Ir). Visually comparing antigen labeling and tissue morphology, we observed no difference in DNA or antibody staining between tissue stained with QMTe and tissue stained with the ^{175}Lu MaxPar secondary antibody, demonstrating that QMTe staining does not perturb the binding of other antibodies or the DNA stain. Furthermore, the morphology of CAIX stained by QMTe is visually comparable to the morphology of CAIX stained by MaxPar, suggesting that any loss of spatial precision by signal amplification is below the 1 μm resolution of the IMC instrument (Figure 4).

In conclusion, we report herein a novel organotellurium reagent for IMC using a secondary detection method. QMTe seamlessly integrates with the current IMC workflow, allowing access to mass channels orthogonal to the current inventory of MC imaging reagents. By using AP turnover, QMTe was observed to give amplifications of 100-fold relative to traditional IMC stains. Further increases in signal can be realized through the generation of isotopically enriched QMTe reagents and potentially through optimization of the amplification protocol for specific tissues and the epitope in question. The improved signals observed may be particularly useful when quantifying low-abundance antigens. Similar to any IHC stains, measurements using QMTe should be further validated by including proper antigen standards during tissue ablations. Furthermore, QMTe can be employed as a universal stain with an AP-secondary antibody conjugate to explore new antigens prior to developing new MaxPar reagents.

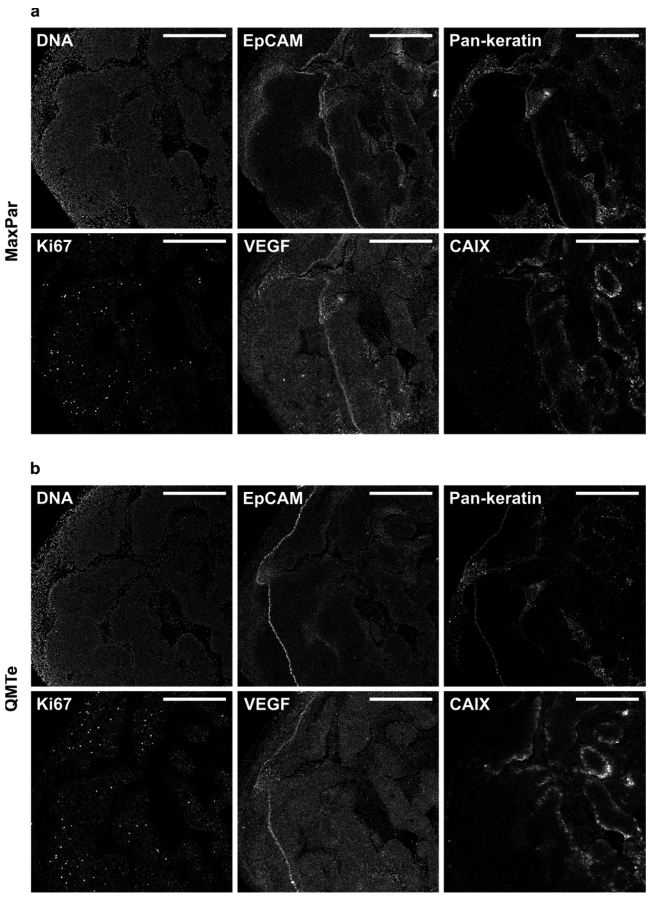

Figure 4. QMTe is compatible with a typical IMC workflow. Five channels from a traditional IMC analysis of HCT116 tumor xenograft are shown: DNA (^{193}Ir), EpCAM (^{144}Nd), pan-keratin (^{162}Dy), Ki67 (^{168}Er), and VEGF (^{163}Dy). CAIX is shown by either (a) MaxPar secondary detection (^{175}Lu) or (b) QMTe (^{125}Te). Scale bars 500 μm.

■ ASSOCIATED CONTENT

Supporting Information

The Supporting Information is available free of charge on the ACS Publications website at DOI: 10.1021/acs.bioconjchem.9b00559.

General experimental details, synthetic procedures, NMR and MS characterization, enzyme kinetics, LC-MS traces, slide staining procedures, data acquisition, and data analysis methods (PDF)

Unprocessed IMC image files have been deposited in the Open Science Framework, https://osf.io/unhzj/.

■ AUTHOR INFORMATION

Corresponding Author

*E-mail: mark.nitz@utoronto.ca.

ORCID

Mark Nitz: 0000-0001-8078-2265

Notes

Imaging Mass Cytometry, IMC, and Maxpar are trademarks and/or registered trademarks of Fluidigm Corporation in the United States and/or other countries. For Research Use Only. The authors declare the following competing financial interest(s): J.B. owns stock in BIMDAQ Ltd. M.N. owns IP on the use of Tellurium in MC.

DOI: 10.1021/acs.bioconjchem.9b00559
Bioconjugate Chem. XXXX, XXX, XXX−XXX

■ ACKNOWLEDGMENTS

We thank T. Closson (Fluidigm) for assistance with IMC. We are grateful to H. Soor (University of Toronto) for LCMS experiments and to Bradly G. Wouters and Ravi N. Vellanki for providing mounted tissue samples. This work was supported by the Natural Sciences and Engineering Research Council, Ontario Centres of Excellence and Fluidigm Canada.

■ REFERENCES

(1) Tanner, S. D., Bandura, D. R., Ornatsky, O., Baranov, V. I., Nitz, M., and Winnik, M. A. (2008) Flow Cytometer with Mass Spectrometer Detection for Massively Multiplexed Single-Cell Biomarker Assay. *Pure Appl. Chem. 80* (12), 2627−2641.

(2) Bandura, D. R., Baranov, V. I., Ornatsky, O. I., Antonov, A., Kinach, R., Lou, X., Pavlov, S., Vorobiev, S., Dick, J. E., and Tanner, S. D. (2009) Mass Cytometry: Technique for Real Time Single Cell Multitarget Immunoassay Based on Inductively Coupled Plasma Time-of-Flight Mass Spectrometry. *Anal. Chem. 81* (16), 6813−6822.

(3) Ornatsky, O., Bandura, D., Baranov, V., Nitz, M., Winnik, M. A., and Tanner, S. (2010) Highly Multiparametric Analysis by Mass Cytometry. *J. Immunol. Methods 361*, 1−20.

(4) Giesen, C., Wang, H. A. O., Schapiro, D., Zivanovic, N., Jacobs, A., Hattendorf, B., Schüffler, P. J., Grolimund, D., Buhmann, J. M., Brandt, S., et al. (2014) Highly Multiplexed Imaging of Tumor Tissues with Subcellular Resolution by Mass Cytometry. *Nat. Methods 11* (4), 417−422.

(5) Singh, M., Chaudhry, P., Gerdtsson, E., Maoz, A., Cozen, W., Hicks, J., Kuhn, P., Gruber, S., Siddiqui, I., and Merchant, A. (2017) Highly Multiplexed Imaging Mass Cytometry Allows Visualization of Tumor and Immune Cell Interactions of the Tumor Microenvironment in FFPE Tissue Sections. *Blood 130*, 2751.

(6) Chang, Q., Ornatsky, O. I., Siddiqui, I., Straus, R., Baranov, V. I., and Hedley, D. W. (2016) Biodistribution of Cisplatin Revealed by Imaging Mass Cytometry Identifies Extensive Collagen Binding in Tumor and Normal Tissues. *Sci. Rep. 6*, 1−11.

(7) Schulz, D., Zanotelli, V. R. T., Fischer, J. R., Schapiro, D., Engler, S., Lun, X., Jackson, H. W., and Bodenmiller, B. (2018) Simultaneous Multiplexed Imaging of MRNA and Proteins with Subcellular Resolution in Breast Cancer Tissue Samples by Mass Cytometry Article Simultaneous Multiplexed Imaging of MRNA and Proteins with Subcellular Resolution in Breast Cancer Tissue Samples b. *Cell Syst. 6* (1), 25−36.

(8) Bendall, S. C., Simonds, E. F., Qiu, P., Amir, E. D., Krutzik, P. O., Finck, R., Bruggner, R. V., Melamed, R., Trejo, A., Ornatsky, O. I., et al. (2011) Single-Cell Mass Cytometry of Differential Immune and Drug Responses Across a Human Hematopoietic Continuum. *Science 332* (6030), 687−696.

(9) Han, G., Chen, S. Y., Gonzalez, V. D., Zunder, E. R., Fantl, W. J., and Nolan, G. P. (2017) Atomic Mass Tag of Bismuth-209 for Increasing the Immunoassay Multiplexing Capacity of Mass Cytometry. *Cytometry, Part A 91A*, 1150−1163.

(10) Han, G., Spitzer, M. H., Bendall, S. C., Fantl, W. J., and Nolan, G. P. (2018) Metal-Isotope-Tagged Monoclonal Antibodies for High-Dimensional Mass Cytometry. *Nat. Protoc. 13*, 2121−2148.

(11) Behbehani, G. K., Bendall, S. C., Clutter, M. R., Fantl, W. J., and Nolan, G. P. (2012) Single-Cell Mass Cytometry Adapted to Measurements of the Cell Cycle. *Cytometry, Part A 81A*, 552−566.

(12) Fienberg, H. G., Simonds, E. F., Fantl, W. J., Nolan, G. P., and Bodenmiller, B. (2012) A Platinum-Based Covalent Viability Reagent for Single-Cell Mass Cytometry. *Cytometry, Part A 81A*, 467−475.

(13) Park, H., Edgar, L. J., Lumba, M. A., Willis, L. M., and Nitz, M. (2015) Organotellurium Scaffolds for Mass Cytometry Reagent Development. *Org. Biomol. Chem. 13*, 7027−7033.

(14) Edgar, L. J., Vellanki, R. N., McKee, T. D., Hedley, D., Wouters, B. G., and Nitz, M. (2016) Isotopologous Organotellurium Probes Reveal Dynamic Hypoxia In Vivo with Cellular Resolution. *Angew. Chem., Int. Ed. 55*, 13159−13163.

(15) Bassan, J., Willis, L. M., Vellanki, R. N., Nguyen, A., Edgar, L. J., Wouters, B. G., and Nitz, M. (2019) TePhe Paper. *Proc. Natl. Acad. Sci. U. S. A. 116*, 8155−8160.

(16) Lumba, M. A., Willis, L. M., Santra, S., Rana, R., Schito, L., Rey, S., Wouters, B. G., and Nitz, M. (2017) A β-Galactosidase Probe for the Detection of Cellular Senescence by Mass Cytometry. *Org. Biomol. Chem. 15*, 6388−6392.

(17) Pichaandi, J., Zhao, G., Bouzekri, A., Lu, E., Ornatsky, O., Baranov, V., Nitz, M., and Winnik, M. A. (2019) Lanthanide Nanoparticles for High Sensitivity Multiparameter Single Cell Analysis. *Chem. Sci. 10*, 2965−2974.

(18) Ponder, B. A., and Wilkinson, M. M. (1981) Inhibition of Endogenous Tissue Alkaline Phosphatase with the Use of Alkaline Phosphatase Conjugates in Immunohistochemistry. *J. Histochem. Cytochem. 29*, 981−984.

(19) Yam, L. T., Khansur, T., and Tavassoli, M. (1988) New Developments in Immunochemistry with Immunoalkaline Phosphatase Methods. *Pathol. Immunopathol. Res. 7*, 169−186.

(20) Wang, Q., Dechert, U., Jirik, F., and Withers, S. G. (1994) Suicide Inactivation of Human Prostatic Acid Phosphatase and a Phosphotyrosine Phosphatase. *Biochem. Biophys. Res. Commun. 200*, 577−583.

(21) Loubinoux, B., Miazimbakana, J., and Gerardin, P. (1989) Reactivity of New Precursors of Quinone Methides. *Tetrahedron Lett. 30*, 1939−1942.

(22) Kumar, S., Zhou, B., Liang, F., Wang, W.-Q., Huang, Z., and Zhang, Z.-Y. (2004) Activity-Based Probes for Protein Tyrosine Phosphatases. *Proc. Natl. Acad. Sci. U. S. A. 101*, 7943−7948.

(23) Lo, L.-C., Pang, T.-L., Kuo, C.-H., Chiang, Y.-L., Wang, H.-Y., and Lin, J.-J. (2002) Design and Synthesis of Class-Selective Activity Probes for Protein Tyrosine Phosphatases. *J. Prot. Res. 1* (1), 35−40.

(24) Lo, L.-C., Chiang, Y.-L., Kuo, C.-H., Liao, H.-K., Chen, Y.-J., and Lin, J.-J. (2004) Study of the Preferred Modification Sites of the Quinone Methide Intermediate Resulting from the Latent Trapping Device of the Activity Probes for Hydrolases. *Biochem. Biophys. Res. Commun. 326* (1), 30−35.

(25) Chen, G. Y. J., Uttamchandani, M., Zhu, Q., Wang, G., and Yao, S. Q. (2003) Developing a Strategy for Activity-Based Detection of Enzymes in a Protein Microarray. *ChemBioChem 4*, 336−339.

(26) Zhu, Q., Huang, X., Chen, G. Y. J., and Yao, S. Q. (2003) Activity-Based Fluorescent Probes That Target Phosphatases. *Tetrahedron Lett. 44*, 2669−2672.

(27) Ahmed, V., Liu, Y., and Taylor, S. D. (2009) Multiple Pathways for the Irreversible Inhibition of Steroid Sulfatase with Quinone Methide-Generating Suicide Inhibitors. *ChemBioChem 10*, 1457−1461.

(28) Polaske, N. W., Kelly, B. D., Ashworth-Sharpe, J., and Bieniarz, C. (2016) Quinone Methide Signal Amplification: Covalent Reporter Labeling of Cancer Epitopes Using Alkaline Phosphatase Substrates. *Bioconjugate Chem. 27*, 660−666.

(29) Kwan, D. H., Chen, H.-M., Ratananikom, K., Hancock, S. M., Watanabe, Y., Kongsaeree, P. T., Samuels, A. L., and Withers, S. G. (2011) Self-Immobilizing Fluorogenic Imaging Agents of Enzyme Activity. *Angew. Chem., Int. Ed. 50*, 300−303.

(30) Lo, L.-C., Lo, C.-H. L., Janda, K. D., Kassel, D. B., and Raushel, F. M. (1996) A Versatile Mechanism Based Reaction Probe for the Direct Selection of Biocatalysts. *Bioorg. Med. Chem. Lett. 6*, 2117−2120.

(31) Lenger, J., Schröder, M., Ennemann, E. C., Müller, B., Wong, C. H., Noll, T., Dierks, T., Hanson, S. R., and Sewald, N. (2012) Evaluation of Sulfatase-Directed Quinone Methide Traps for Proteomics. *Bioorg. Med. Chem. 20*, 622−627.

(32) Seaman, M. E., and Kelly, K. A. S. (2013) *Cancer Res. 73*, 3891.

(33) Gutknecht, M. F., Seaman, M. E., Ning, B., Cornejo, D. A., Mugler, E., Antkowiak, P. F., Moskaluk, C. A., Hu, S., Epstein, F. H., and Kelly, K. A. (2017) Identification of the S100 Fused-Type Protein Hornerin as a Regulator of Tumor Vascularity. *Nat. Commun. 8*, 552.

(34) McIntyre, A., Patiar, S., Wigfield, S., Li, J. -l., Ledaki, I., Turley, H., Leek, R., Snell, C., Gatter, K., Sly, W. S., et al. (2012) Carbonic

DOI: 10.1021/acs.bioconjchem.9b00559
Bioconjugate Chem. XXXX, XXX, XXX−XXX

Anhydrase IX Promotes Tumor Growth and Necrosis In Vivo and Inhibition Enhances Anti-VEGF Therapy. *Clin. Cancer Res. 18*, 3100−3111.

(35) Wykoff, C. C., Beasley, N. J. P., Watson, P. H., Turner, K. J., Pastorek, J., Sibtain, A., Wilson, G. D., Turley, H., Talks, K. L., Maxwell, P. H., et al. (2000) Hypoxia-Inducible Expression of Tumor-Associated Carbonic Anhydrases. *Cancer Res. 60*, 7075−7083.

DOI: 10.1021/acs.bioconjchem.9b00559
Bioconjugate Chem. XXXX, XXX, XXX−XXX